https://doi.org/10.20965/jdr.2019.p0456

Paper:

Building Damage Assessment Using Intensity SAR Data with Different Incidence Angles and Longtime Interval

Pinglan Ge[*,†], **Hideomi Gokon**[**], **and Kimiro Meguro**[**]

[*]Graduate School of Engineering, The University of Tokyo
4-6-1 Komaba, Meguro-ku, Tokyo 153-8505, Japan
[†]Corresponding author, E-mail: gepl@iis.u-tokyo.ac.jp
[**]Institute of Industrial Science, The University of Tokyo, Tokyo, Japan
[Received October 31, 2018; accepted January 29, 2019]

When carrying out change detection for building damage assessment using synthetic aperture radar (SAR) intensity images, it is desirable that the observation conditions of the images are similar and acquisition time is close to the earthquake occurrence time. In this way, the influence of the radar operating system and ground temporal changes can be minimized, facilitating high-accuracy assessment results. However, in practice, especially in poor developing areas, it is difficult to obtain ideal images owing to limited pre-event data archives. In the 2015 Gorkha, Nepal earthquake, the TerraSAR-X satellite captured the influenced Sankhu area before and after the earthquake on May 30, 2010 and May 13, 2015, respectively. The pre-event data was obtained in an ascending path with an incidence angle of 41°, whereas the post-event data was obtained in a descending path with an incidence angle of 33°. To apply the obtained data that had different observation conditions and longtime intervals for building damage assessment, two ways were considered and studied. On one hand, the feasibility of change detection considering these factors was investigated. Pixel statistic characteristics were analyzed in twelve test areas to check the influence of temporal changes, and building footprints were buffered considering two different incidence angles. On the other hand, the reliability of classification based on only post-event data was studied. The results showed good classification performance of some texture parameters, such as the "range value" and "standard deviation," which are worthy of further study. Moreover, the classification results obtained using the post-event data achieved similar accuracy to that using both the pre- and post-event data, preliminarily indicating the research value of post-event data-based building damage detection as it can solve the pre-event data limitation problem once and for all.

Keywords: synthetic aperture radar (SAR), building damage assessment, incidence angle, longtime interval, random forest

1. Introduction

Synthetic aperture radar (SAR) is a useful tool for emergency response in disasters, such as in promptly identifying the most damaged urban areas and reasonably arranging rescue forces, because of its all-weather and all-time working capabilities. Various SAR-based approaches for damage assessment (particularly building damage assessment) in disasters have been proposed with the development of microwave remote sensing technology. Depending on the data availability, resolution conditions, and acquisition mode, the approaches vary from those applying pre- and post-event data [1, 2] to those utilizing only post-event data [3–5], from those in block-units [6–9] to those in building-units [10, 11], from those carrying out physical relationship analysis to those employing machine learning technology [12], and from those using intensity analysis to those using coherence [13, 14] and polarimetry analysis [15].

When a SAR satellite does not work in an interferometry or polarimetry mode, only the intensity value of the pixels can provide useful information for damage assessment. Intensity means the backscattering received by the SAR sensor after sending microwaves to ground targets. Change detection using pre- and post-disaster intensity SAR data in a block-unit or a building-unit is a classic and commonly-used method. It is based on the following principle: for an intact building, owing to the oblique view of the SAR satellite, ideally, regular layover and shadow areas appear in the SAR image. In areas facing the radar sensor, a bright zone appears owing to a double bounce effect in the corner and superposition of the roof, wall, and ground reflections. In most areas of the building footprints and some areas facing backward to the radar sensor, a shadow zone appears owing to the occlusion of the building (**Fig. 1**). For a collapsed building, however, the layover, double bounce, and even shadow characteristics may disappear, making the overall reflection around the building more random and averaged. Therefore, based on differences of pixel statistic characteristics such as backscattering difference, texture variation, and bright area percentage change, it is possible to distinguish between damaged and undamaged buildings.

Backscattering coefficients of SAR can be influenced

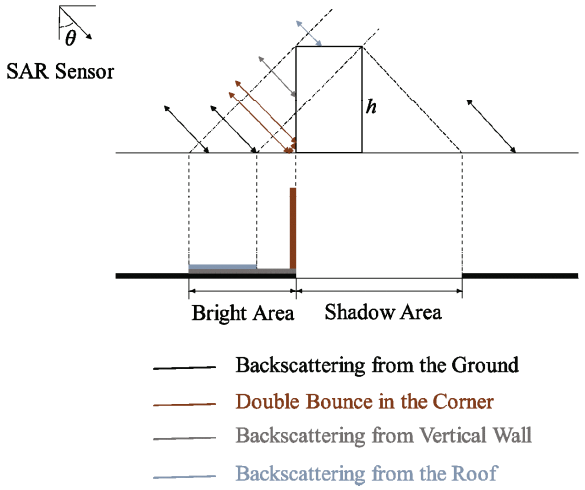

Fig. 1. Schematic of intact building backscattering in SAR.

by characteristics of ground targets (roughness, dielectric, etc.) and operating parameters of the radar system (wavelength, incidence angle, etc.). Therefore, when carrying out change detection, it is desirable that the acquisition dates of the images are as close as possible to the day of the earthquake and that the observation conditions are similar [16]. However, in reality, owing to the limited archives of pre-event SAR data [17], it is not easy to obtain ideal images, especially in poor developing areas. For the 2015 Gorkha, Nepal earthquake, the TerraSAR-X satellite captured the influenced Sankhu area before the disaster on May 30, 2010, and after the disaster on May 13, 2015. Whereas the pre-event image was obtained in an ascending path with a central incidence angle of 41°, the post-event image was obtained in a descending path with a central incidence angle of 33°. The long data acquisition interval provided time for temporal changes on the earth's surface and buildings, interfering with the damage assessment results. The difference of radar path and incidence angle made pixel-by-pixel comparison lose clear physical meaning, as a pixel in the same coordinate might not represent the same ground target anymore. Moreover, even for the same ground target, the radar backscattering return was also different at different incidence angles. Wagner et al. revealed that the backscattering is stronger at smaller incidence angles, and the rate of decrease depends on roughness conditions and land cover [18].

To apply the obtained data with different observation conditions and a longtime interval for building damage assessment, two methods can be considered. On one hand, the feasibility of change detection considering these influencing factors can be analyzed. On the other hand, if good classification results can be achieved by using only post-event data, then the limitation of the pre-event data will no longer be a problem. In this study, firstly, the feasibility of change detection was checked. Pixel statistic characteristics were analyzed in twelve test areas, to check the influence of temporal changes and choose better parameters for classification. Building footprints were buffered according to the relationship between the incidence angle and the length of layover and shadow region, to incorporate all bright and dark areas. Random forest classification was then applied based on the selected parameters calculated for each building within the buffered areas. To study the cost-efficiency of the selected parameters, classification using all parameters was also executed for comparison. To investigate the reliability of the post-event data-based method, classification using similar parameters calculated from post-event data was carried out and compared.

2. Research Area and Dataset

The 2015 Gorkha, Nepal earthquake, with a moment magnitude of 7.8 (Mw), occurred on April 25, 2015, causing heavy casualties and serious economic losses. The hypocenter of the earthquake located in 28.15°N, 84.71°E with a depth of 15 km (USGS).

After the main shock, more than 25 aftershocks occurred, among which, at 27.82°N, 86.08°E, a 7.3 magnitude major shock occurred on May 12, 2015 with a depth of 19 km (USGS). According to the Nepal Police, in the earthquake, 8,832 people were killed, 25,422 people were injured and more than 5,000,000 houses were damaged [19].

Sankhu, the study area of this research, was a region extensively damaged in the earthquake. It was an old town, located in the northeast part of the Kathmandu Valley (**Fig. 2(a)**), where there were around one thousand buildings. Among all the buildings, the non-engineered masonry buildings experienced considerable damage, whereas the reinforced concrete (RC) buildings encountered minor damage [19].

Pre- and post-event TerraSAR-X images were obtained on May 30, 2010 and May 13, 2015, respectively. The spatial resolution of the images was around 3 m. The acquisition mode was Stripmap and the polarization mode was horizontal transmit/horizontal receive (HH). The pre-event image was acquired in an ascending path with a central incidence angle of 41°, whereas the post-event image was acquired in a descending path with a central incidence angle of 33°. High-resolution optical images from March 12, 2015 (before the earthquake) and November 20, 2015 (after the earthquake) could be obtained via Google Earth. These images were used to create building footprints and a damage map (**Fig. 2(b)**) based on visual interpretation. The damage level (**Table 1**) made for the Nepal Earthquake Risk Assessment System [20] considering the overall building damage of HAZUS [21] and the component damage level of FEMA-306 [22] was used to define the damaged and undamaged buildings in this study. Buildings in the complete damage state were identified as damaged, while buildings in the damage states of slight, moderate, and extensive were defined as undamaged.

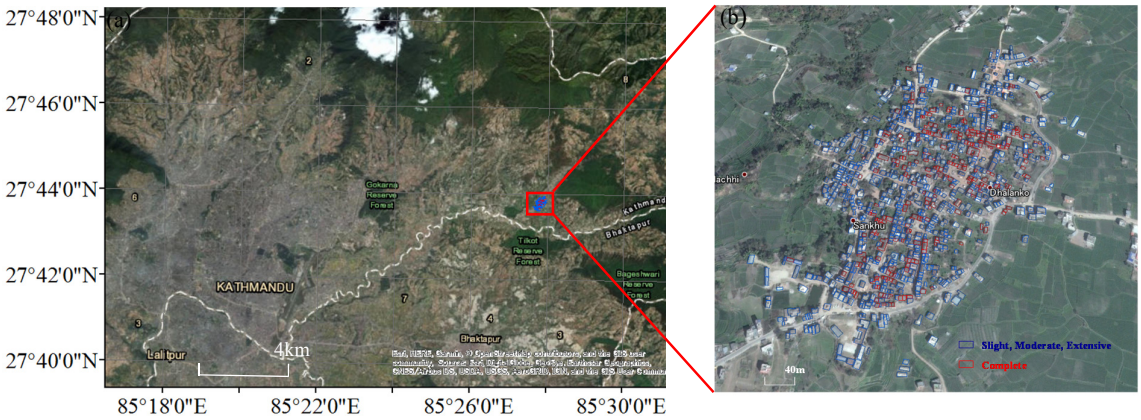

Fig. 2. Study area and corresponding building damage map: (a) location of Sankhu area; (b) building damage map.

Table 1. Definition of damage level.

Damage State	Damage Definition
Slight	Diagonal, stair-step hairline cracks on masonry wall surfaces; larger cracks around door and window openings in walls with large proportion of openings; movements of lintels; cracks at the base of parapets.
Moderate	Most wall surfaces exhibit diagonal cracks; some of the walls exhibit larger diagonal cracks; masonry walls may have visible separation from diaphragms; significant cracking of parapets; some masonry may fall from walls or parapets.
Extensive	In buildings with relatively large area of wall openings most walls have suffered extensive cracking. Some parapets and gable end walls have fallen. Beams or trusses may have moved relative to their supports.
Complete	Structure has collapsed or is in imminent danger of collapse due to in-plane or out-of-plane failure of the walls. Approximately 15% of the total area of URM buildings with complete damage is expected to be collapsed.

3. Methodology

3.1. Principal

As explained in the introduction, for an intact building, layover and shadow regions exist, forming regular bright and dark areas in the SAR image. For the collapsed building, however, the layover, double bounce, and even shadow characteristics may disappear, averaging the total reflection in and around the building. Therefore, for collapsed buildings, ideally, pixel statistic characteristics around the building areas would have some specific changes. For example, the minimum pixel value would become greater because of the disappear of shadow areas, the maximum pixel value would become smaller because of the vanish of the double bounce, the pixel value range and standard deviation would become smaller owing to the average of the overall backscattering.

However, in the case of this study, temporal changes might occur during the longtime interval between the pre- and post-event image acquisition date, interfering with the regularities of these changes. Thus, before using these pixel statistic parameters for classification, twelve test areas, with six damaged ones and six undamaged ones were selected to check the change trends and choose better parameters for classification.

To consider the influence of different observation conditions, the building footprints were buffered, considering the two different incidence angles. The physical relationship between the incidence angle and the length of layover and shadow regions was analyzed to determine the buffer range. As can be seen from the reflection law in **Fig. 1**, the layover and shadow length was approximately $h/\tan\theta$ and $h\tan\theta$ (h is the height of the building and θ is the incidence angle), respectively. Therefore, to incorporate all of the shadow, double bounce, and layover effects, the maximum value among $h/\tan\theta_{pre}$, $h\tan\theta_{pre}$, $h/\tan\theta_{post}$, and $h\tan\theta_{post}$ was set as the buffer distance. The building height h was estimated approximately according to the story information described by Ohsumi et al. through field survey [19].

After classification parameters were selected and building footprints were buffered, the selected parameters were calculated for each building within the buffered areas, and the random forest algorithm was applied for building damage discrimination based on these calculated parameters.

3.2. Pre-Processing

Pre-processing included radiometric calibration, de-speckling, and registration. Firstly, radiometric calibration, i.e., transforming the image pixel values (or digital number (DN)) into sigma naught (dB), was carried out according to Eq. (1) to minimize the differences in the image radiometry. Then, de-speckling was executed by a 3×3 pixel Lee filter [23] to reduce the noise interference while retaining detailed surface information. Finally, the

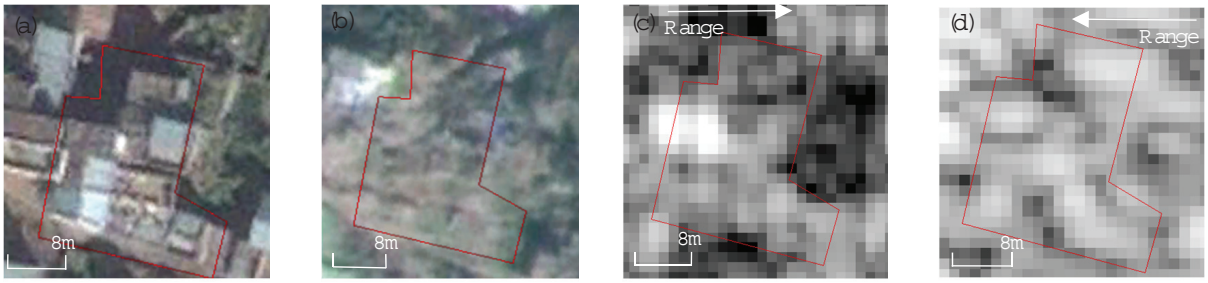

Fig. 3. An example of selected areas with damaged buildings: (a) pre-event optical image; (b) post-event optical image; (c) pre-event SAR image; (d) post-event SAR image.

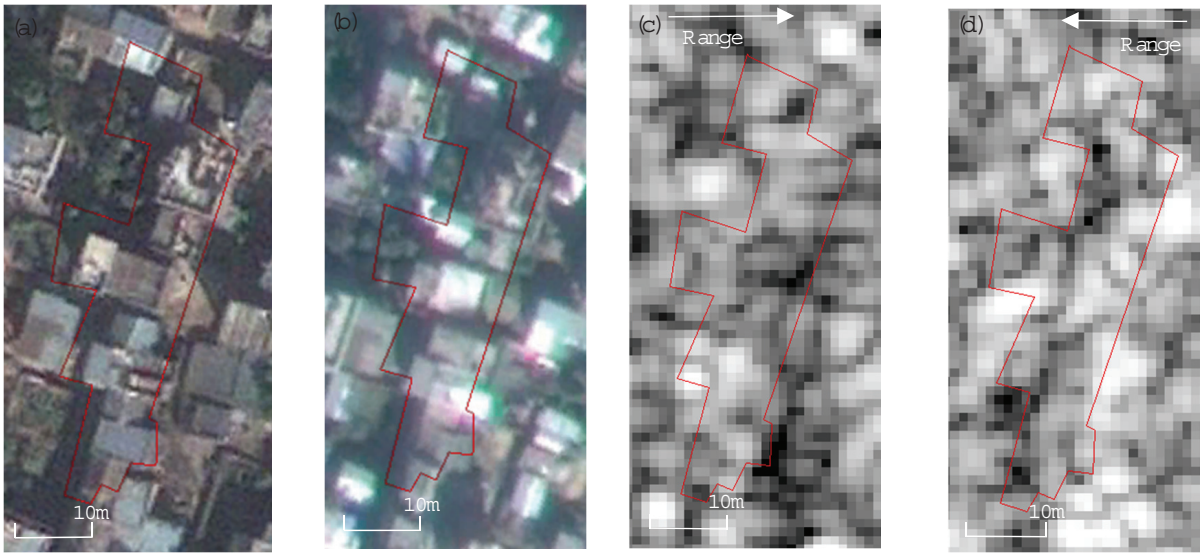

Fig. 4. An example of selected areas with undamaged buildings: (a) pre-event optical image; (b) post-event optical image; (c) pre-event SAR image; (d) post-event SAR image.

two SAR images and the building footprints were all projected to WGS 1984 / UTM zone 45N reference for calculation and analysis.

$$\sigma^0 = \left(k_s \cdot |DN|^2 - NEBN\right) \cdot \sin\theta_{loc} \quad . \quad . \quad . \quad . \quad (1)$$

In Eq. (1), k_s is the calibration and processor scaling factor given by the parameter calFactor in the attached annotated file, DN is the pixel intensity values – digital number in the image, NEBN is the noise equivalent beta naught, θ_{loc} is the local incidence angle, which can be obtained from the GIM in the Enhanced Ellipsoid Corrected (EEC) product.

3.3. Parameter Study

To check the influence of temporal changes on pixel statistic characteristics and to choose better parameters for building damage classification, twelve regions were selected, with six regions full of damaged buildings and six regions full of undamaged buildings. Examples of the selected areas are shown in **Figs. 3** and **4**. The lines in the images denote the outline of the selected damaged or undamaged sample areas. Comparing the pre- and post-event SAR images in **Figs. 3(c)** and **3(d)**, it can be seen that after the damage of the buildings, the overall pixel values seem to become more uniform. To observe the pixel statistic characteristics change of the damaged areas intuitively, the distribution of seven statistical parameters were investigated and analyzed, including the post-pre difference of the minimum value, maximum value, range, mean, standard deviation, skewness, and kurtosis. Parameter values were calculated within each selected area by ArcGIS 10.5. Value distributions were drawn in **Fig. 5** for easier analysis.

As it can be seen from **Fig. 5**, among all parameters, the distribution of the minimum value difference, range difference, and standard deviation difference show different ranges for damaged and undamaged areas, indicating their better classification abilities for building damage conditions. To show the data distribution more clearly, boxplot figures of the three parameters were drawn by python 3.6 (**Fig. 6**). From **Fig. 6**, it can be seen that for the damaged condition, in general, the minimum value difference is larger than zero, whereas the range difference

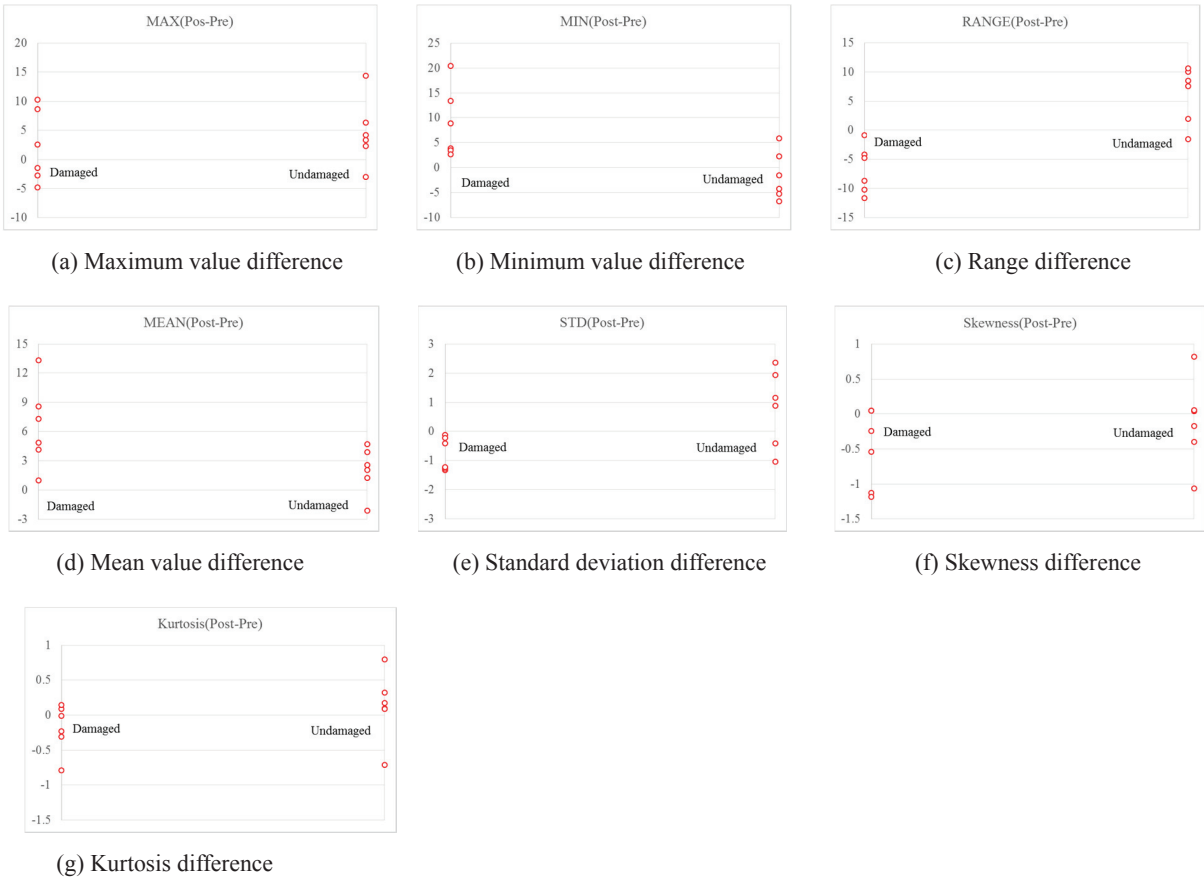

(a) Maximum value difference (b) Minimum value difference (c) Range difference

(d) Mean value difference (e) Standard deviation difference (f) Skewness difference

(g) Kurtosis difference

Fig. 5. Distribution of pixel statistic characteristics for damaged and undamaged test areas.

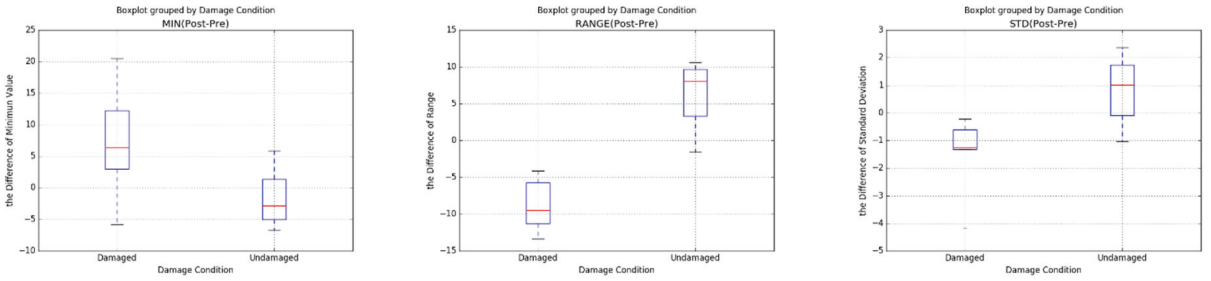

(a) Minimum value difference (b) Range difference (c) Standard deviation difference

Fig. 6. Boxplot of minimum value difference, range difference, and standard deviation difference.

and standard deviation difference are smaller than zero. This implies that the minimum pixel value became bigger, whereas the pixel range and standard deviation became smaller after the buildings were damaged, consistent with the speculation in the desirable condition. Therefore, even though temporal changes might happen during the long pre- and post-event data acquisition interval, these three parameters still had good classification abilities and could be used for identifying damaged and undamaged buildings in this case.

3.4. Machine Learning Based Damage Classification Using Pre- and Post-Event Data

According to the parameter analysis in Section 3.3, the differences of minimum value, range, and standard deviation had better abilities for distinguishing damaged and undamaged areas in this case, and thus were selected as the classification parameters. Then, building footprints were buffered, considering two different incidence angles, to incorporate all shadow, layover, and double bounce effects. Selected parameters were calculated for each building within the buffered areas.

The random forest algorithm was applied as the clas-

Table 2. Classification results using all parameters based on pre- and post-event data.

		Undamaged	Damaged	P.A. (Producer's Accuracy)
GTD (Ground Truth Data)	Undamaged	670	68	90.80%
	Damaged	222	44	16.50%
U.A. (User's Accuracy)		75.1%	39.3%	
O.A. (Overall Accuracy)		71.1%		

Table 3. Classification results using selected parameters based on pre- and post-event data.

		Undamaged	Damaged	P.A.
GTD	Undamaged	651	87	88.2%
	Damaged	207	59	22.22%
U.A.		75.9%	40.4%	
O.A.		70.7%		

sifier, after testing many machine learning methods. 10-fold cross-validation, which means ten equal-size samples were proportionally and randomly divided with nine subsamples applied as training data and the remaining one applied as validation data, was used to check how well the training model could be generalized to independent testing data.

To investigate the classification ability of the selected parameters and ascertain the influence of other parameters, random forest classification using all of the seven parameters was carried out for comparison. Results are shown in **Tables 2** and **3**. Corresponding damage map results are shown in **Figs. 7(b)** and **7(c)**.

As shown in **Tables 2** and **3**, the overall accuracy of the classification is around 70%, which is not a very bad result. It demonstrates that even though the pre- and post-event data are not desirable, change detection can still be carried out by conducting test studies to ascertain the influence factors as well as the change trends carefully, and then considering various influencing factors reasonably.

Moreover, the overall accuracy of the classification based on the selected parameters and that of the classification based on all parameters are generally the same. This implies that the integration of other parameters cannot efficiently improve the classification results, the selected parameters already have favorable and cost-effective classification abilities in this case. Actually, considering too many parameters, especially the bad and irregular ones, might cause interference and overfitting issues in the training process. Moreover, according to **Tables 2** and **3**, the classification accuracy for undamaged buildings is improved while that for damaged buildings is reduced when other parameters were taken into account. This may imply that the selected parameters are better at discriminating damaged buildings, whereas others are better at identifying undamaged buildings.

3.5. Machine Learning Based Damage Classification Using Only Post-Event Data

According to the reflection law of intact and collapsed buildings, pixel statistic characteristics of the damaged and undamaged buildings in the post-event image should also have some differences. By analyzing these differences, perhaps the damage conditions of buildings could be discriminated by only using the post-event data.

To analyze pixel statistic characteristic differences between damaged and undamaged buildings in the post-event image, a parameter study was carried out, in the same way as Section 3.3. Analysis results showed that the minimum value, range, and standard deviation still had better performance for differentiating between damaged and undamaged buildings. Therefore, based on these three parameters, random forest classification using only post-event data was executed. The classification damage map result is shown in **Fig. 7(d)**, and the accuracy is listed in **Table 4**.

As can be seen from **Tables 3** and **4**, using only post-event data does not reduce the classification accuracy, and on the contrary, seems to improve the accuracy slightly, especially for discriminating damaged buildings. Combined with the research of Bai et al. [12], it can be concluded that, either for a long interval condition or for a short interval condition, methods using only post-event data could achieve almost as good of results as those using multi-temporal data. Moreover, owing to the fact that approaches using only post-event data could settle the pre-event data limitation problem once and for all, it is worth carrying out corresponding research further.

4. Results and Discussion

As shown in **Tables 2–4**, the accuracy of the classification results is not quite high, especially for the damaged buildings, many of which are classified as undamaged ones. Possible underlying factors for the misclassification are analyzed as follows.

Firstly, there is a long interval between the pre- and post-event data. Even though for the selected test areas, the temporal changes do not significantly interfere the classification abilities of the selected parameters, other places may experience changes of a different degree. In addition, repair, new construction, and reconstruction

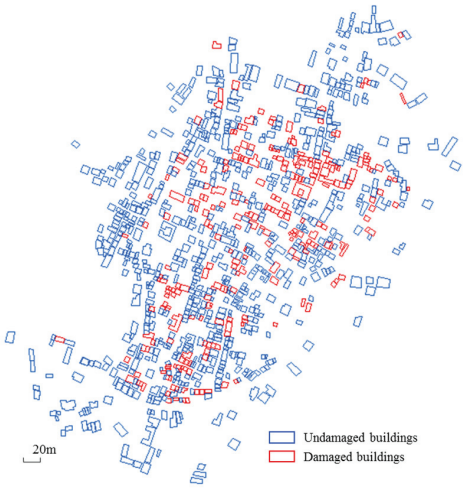

(a) Damage mapping made by Google Earth optical images

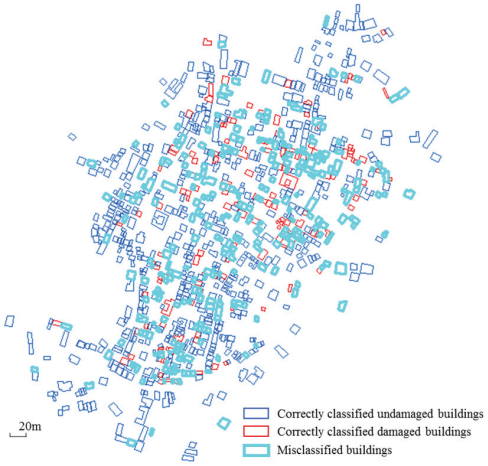

(b) Damage mapping result using pre- and post-event data (all parameters)

(c) Damage mapping result using pre- and post-event data (selected parameters)

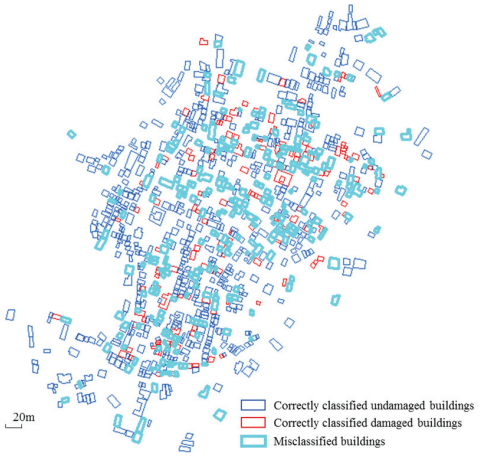

(d) Damage mapping result using only post-event data (selected parameters)

Fig. 7. Building damage map.

Table 4. Classification results using selected parameters based on only post-event data.

		Undamaged	Damaged	P.A.
GTD	Undamaged	653	85	88.5%
	Damaged	198	68	25.6%
U.A.		76.7%	44.4%	
O.A.		71.8%		

of houses might occur during the interval period. For example, when comparing the optical images of 2010 and 2015, approximately 40 buildings were found to be newly-constructed in the studied Sankhu area. The existence of such impact factors would consequentially interfere with the training process in machine learning, and thus influence the classification accuracy.

Secondly, the ground truth damage map was made from optical images in Google Earth that might not be as accurate as damage data obtained through a field survey. Misclassification in the ground truth data generates a mismatch between the damage condition and relevant pixel statistic parameters, misleading the learning process in the machine learning algorithm.

Moreover, data imbalance exists between the damaged and undamaged buildings. There are relatively fewer damaged buildings as compared with undamaged buildings, which may lead to insufficient training for the damage condition, and cause low accuracy in the damaged building classification. Moreover, as the classification pa-

rameters were calculated within buffered building footprint areas, the density of buildings will also have an impact on the classification results.

Furthermore, according to Miura et al. [24], in high-resolution SAR images, the radar reflections could be stronger in a post-event image, especially in a congested building area. However, in the study, this phenomenon was not considered, for simplification of analysis. This unusual intensity change between the pre- and post-event images is also a factor influencing the classification accuracy.

5. Conclusion

In this study, building damage assessment for the 2015 Gorkha, Nepal earthquake was carried out using HH polarimetric TerraSAR-X intensity data. To consider different observation conditions and longtime intervals between the pre- and post-event data, buildings were buffered considering two different angles, and pixel statistic characteristics were analyzed in test areas to find change trends and seek better parameters for classification. After that, selected parameters were calculated for each building within the buffered areas, and the random forest algorithm was applied for classification. In addition, classification results using the selected parameters and all parameters were compared, to study the cost-efficiency of the selected parameters. Sorting outcomes using only post-event data and both pre- and post-event data were weighed to identify the reliability of post-event data-based method. Through this research, several conclusions can be drawn, as follows.

Even though there is a longtime interval between the pre- and post-event data, several pixel statistic parameters (the minimum value difference, range difference, and standard deviation difference) show different distributions for damaged and undamaged buildings, consistent with the speculation in a desirable condition. The good classification abilities of these parameters made them the selected parameters for identifying damage conditions in this case.

Change detection using pre- and post-event intensity SAR data with different observation conditions and longtime intervals is still feasible, by ascertaining the impact factors as well as change trends carefully through test study, and then considering various impact factors reasonably. This also proves that intensity analysis is robust as compared with interferometry analysis, etc.

As compared with other parameters, the selected parameters have favorable and cost-effective capabilities for building damage classification in this case, especially for damaged building discrimination.

Classification using only post-event data can achieve almost the same quality of results as that using both pre- and post-event data, and is worth further research. If more case studies are carried out and show the same reliable results, then the pre-event data limitation problem will be solved once and for all.

Acknowledgements

This research was supported financially by Grants-in-Aid for Scientific Research project numbers 16K20988, the Core Research for Evolutional Science and Technology (CREST) program "Establishing the most advanced disaster reduction management system by fusion of real-time disaster simulation and big data assimilation," and the Ministry of Education, Culture, Sports, Science and Technology (MEXT).

References:

[1] M. Matsuoka and F. Yamazaki, "Characteristics of satellite images of damaged areas due to the 1995 Kobe earthquake," 2nd Conf. on the Applications of Remote Sensing and GIS for Disaster Management, The George Washington University, 1999.

[2] L. An, G. Zhang, L. Gong, and Q. Li, "Integration of SAR image and vulnerability data for building damage degree estimation," 2016 IEEE Int. Geoscience and Remote Sensing Symp. (IGARSS), pp. 4263-4266, 2016.

[3] F. Wu, L. Gong, C. Wang, H. Zhang, B. Zhang, and L. Xie, "Signature analysis of building damage with TerraSAR-X new staring spotlight mode data," IEEE Geoscience and Remote Sensing Letters, Vol.13, No.11, pp. 1696-1700, 2016.

[4] Y. Bai, B. Adriano, E. Mas, H. Gokon, and S. Koshimura, "Object-based building damage assessment methodology using only post event ALOS-2/PALSAR-2 dual polarimetric SAR intensity images," J. Disaster Res., Vol.12, No.2, pp. 259-271, 2017.

[5] Y. Bai, B. Adriano, E. Mas, and S. Koshimura, "Building damage assessment in the 2015 Gorkha, Nepal, earthquake using only post-event dual polarization synthetic aperture radar imagery," Earthquake Spectra, Vol.33, No.S1, pp. 185-195, 2015.

[6] M. Matsuoka and F. Yamazaki, "Building damage detection using satellite SAR intensity images for the 2003 Algeria and Iran earthquakes," Geoscience and Remote Sensing Symp., Vol.2, pp. 1099-1102, 2004.

[7] W. Wen, F. Yamazaki, H. Gokon, and S. Koshimura, "Extraction of tsunami-flooded areas and damaged buildings in the 2011 Tohoku-Oki earthquake from TerraSAR-X intensity images," Earthquake Spectra, Vol.29, No.S1, pp. 183-200, 2013.

[8] H. Gokon, S. Koshimura, and K. Meguro, "Verification of a method for estimating building damage in extensive tsunami affected areas using L-band SAR data," J. Disaster Res., Vol.12, No.2, pp. 251-258, 2017.

[9] H. Gokon, S. Koshimura, and K. Meguro, "Towards a damage assessment in a tsunami affected area using L-band and X-band SAR data," Joint Urban Remote Sensing Event (JURSE), pp. 1-4, 2017.

[10] R. Guida, A. Iodice, and D. Riccio, "An application of the deterministic feature extraction approach to COSMO-SkyMed data," 8th European Conf. on Synthetic Aperture Radar, pp. 1-4, 2011.

[11] H. Gokon, J. Post, E. Stein, S. Martinis, A. Twele, M. Mück, C. Geiß, S. Koshimura, and M. Matsuoka, "A method for detecting buildings destroyed by the 2011 Tohoku earthquake and tsunami using multi-temporal TerraSAR-X data," IEEE Geoscience and Remote Sensing Letters, Vol.12, No.6, pp. 1277-1281, 2015.

[12] Y. Bai, B. Adriano, E. Mas, and S. Koshimura, "Machine learning based building damage mapping from the ALOS-2/PALSAR-2 SAR imagery: case study of 2016 Kumamoto earthquake," J. Disaster Res., Vol.12, No.sp, pp. 646-655, 2017.

[13] M. Watanabe, R. Thapa, T. Ohsumi, H. Fujiwara, C. Yonezawa, N. Tomii, and S. Suzuki, "Detection of damaged urban areas using interferometric SAR coherence change with PALSAR-2," Earth, Planets and Space, Vol.68, No.1, pp. 131, 2016.

[14] D. Oxoli, P. Boccardo, M. Brovelli, E. Molinari, and A. Monti, "Coherent change detecting for repeated-pass interferometric SAR images: an application to earthquake damage assessment on buildings," The Int. Archives of the Photogrammetry, Remote Sensing and Spatial Information Sciences, Vol.XLII-3/W4, pp. 383-388, 2018.

[15] S. Chen, X. Wang, and M. Sato, "Urban damage level mapping based on scattering mechanism investigation using fully polarimetric SAR data for the 3.11 east japan earthquake," The Int. Archives of the Photogrammetry, IEEE Trans. on Geoscience and Remote Sensing, Vol.54, No.12, pp. 6919-6929, 2016.

[16] M. Matsuoka and F. Yamazaki, "Building damage mapping of the 2003 Bam, Iran Earthquake using Envisat/ASAR intensity imagery," Earthquake Spectra, Vol.21, No.S1, pp. 285-294, 2005.

[17] D. Brunner, K. Schulz, and T. Brehm, "Building damage assessment in decimeter resolution SAR imagery: A future perspective," 2011 Joint Urban Remote Sensing Event, pp. 217-220, 2016.

[18] W. Wagner, J. Noll, M. Borgeaud, and H. Rott, "Monitoring soil moisture over the Canadian Prairies with the ERS scatterometer," IEEE Trans. on Geoscience and Remote Sensing, Vol.37, No.1, pp. 206-216, 1999.
[19] T. Ohsumi, Y. Mukai, and H. Fujitani, "Investigation of damage in and around Kathmandu valley related to the 2015 Gorkha, Nepal earthquake and beyond," Geotechnical and Geological Engineering, Vol.34, No.4, pp. 1223-1245, 2016.
[20] R. Guragain, "Development of earthquake risk assessment system for Nepal," Ph.D. Thesis, The University of Tokyo, 2015.
[21] HAZUS, "Multi-hazard Loss Estimation Methodology: Earthquake Model," Department of Homeland Security, Emergency Preparedness and Response Directorate FEMA, Washington D.C., 2003.
[22] FEMA 306, "Evaluation of Earthquake Damaged Concrete and Masonry Wall Buildings - Basic Procedures Manual," prepared by the Applied Technology Council (ATC-43), 1999.
[23] J. Lee, "Digital image enhancement and noise filtering by use of local statistics," IEEE Trans. on Pattern Analysis and Machine Intelligence, Vol.2, No.2, pp. 165-168, 1980.
[24] H. Miura, S. Midorikawa, and M. Matsuoka, "Building Damage Assessment Using High-Resolution Satellite SAR Images of the 2010 Haiti Earthquake," Earthquake Spectra, Vol.32, No.1, pp. 591-610, 2016.

Name:
Pinglan Ge

Affiliation:
Ph.D. Student, Graduate School of Engineering, The University of Tokyo

Address:
Be604, 4-6-1 Komaba, Meguro-ku, Tokyo 153-8505, Japan

Brief Career:
2014-2017 Master Student, College of Civil Engineering, Tongji University
2017-present Ph.D. Student, Graduate School of Engineering, The University of Tokyo

Selected Publications:
• S. Gong, Y. Zhou, and P. Ge, "Seismic analysis for tall and irregular temple buildings: a case study of strong nonlinear viscoelastic dampers," Structural Design of Tall & Special Buildings, 2016.
• Y. Zhou, P. Ge, J. Han, and Z. Lu, "Vector-valued intensity measures for incremental dynamic analysis," Soil Dynamics and Earthquake Engineering, pp. 380-388, 2017.

Name:
Hideomi Gokon

Affiliation:
Assistant Professor, Institute of Industrial Science, The University of Tokyo

Address:
Be604, 4-6-1 Komaba, Meguro-ku, Tokyo 153-8505, Japan

Brief Career:
2012-2015 Doctoral Course Student, Graduate School of Engineering, Tohoku University
2012-2015 JSPS Research Fellow (DC1)
2012 Visiting Researcher of German Aerospace Center (DLR)
2015- Assistant Professor, Institute of Industrial Science, The University of Tokyo

Selected Publications:
• H. Gokon, S. Koshimura, and M. Matsuoka, "Object-based method for estimating tsunami induced damage using TerraSAR-X data," J. Disaster Res., Vol.11, No.2, pp. 225-235, 2016.
• H. Gokon, J. Post, E. Stein, S. Martinis, A. Twele, M. Mück, C. Geiß, S. Koshimura, and M. Matsuoka, "A Method for Detecting Devastated Buildings by the 2011 Tohoku Earthquake Tsunami Using Multi-temporal TerraSAR-X Data," Geoscience and Remote Sensing Letters, IEEE, 2015.
• H. Gokon, S. Koshimura, K. Imai, M. Matsuoka, Y. Namegaya, and Y. Nishimura, "Developing Fragility Functions for the Areas Affected by the 2009 Samoa Earthquake and Tsunami," Natural Hazards and Earth System Sciences, Vol.14, pp. 3231-3241, 2014.

Academic Societies & Scientific Organizations:
• Japan Society of Civil Engineers (JSCE)
• Architectural Institute of Japan (AIJ)
• Japan Association for Earthquake Engineering (JAEE)

Name:
Kimiro Meguro

Affiliation:
Professor, Institute of Industrial Science, The University of Tokyo

Address:
Be604, 4-6-1 Komaba, Meguro-ku, Tokyo 153-8505, Japan

Brief Career:
1991 Research Associate, Institute of Industrial Science, The University of Tokyo
1995 Associate Professor, Institute of Industrial Science, The University of Tokyo
2007 Director of International Center for Urban Safety (ICUS), Institute of Industrial Science, The University of Tokyo
2008 Visiting Professor of The Open University of Japan
2010 Professor, Graduate School of Interdisciplinary Information Studies, The University of Tokyo
2015 Director of the Japan Association for Earthquake Engineering
2016 Special Advisor of Cabinet Office, Government of Japan

Selected Publications:
• M. Kohiyama, A. S. Kiremidjian, K. Meguro, and M. Ohara, "Incentives and Disincentives Analysis for Improving Policy for Seismic Risk Management of Homeowners in Japan," Natural Hazards Review, ASCE, Vol.9, No.4, pp. 170-178, 2008.
• M. Matsuoka and N. Nojima, "Building Damage Estimation by Integration of Seismic Intensity Information and Satellite L-band SAR Imagery," Remote Sensing, MDPI, Vol.2, No.9, pp. 2111-2126, 2010.
• K. Meguro and H. Tagel-Din, "Applied Element Simulation of RC Structure under Cyclic Loading," J. of Structural Engineering, ASCE, Vol.127, No.11, pp. 1295-1305, 2001.

Academic Societies & Scientific Organizations:
• Japan Society of Civil Engineers (JSCE)
• Institute of Social Safety Science
• Japan Association for Earthquake Engineering (JAEE)
• International Association for Earthquake Engineering (IAEE)
• World Seismic Safety Initiative (WSSI)
• Japan Society for Natural Disaster Science
• Japan Society for Active Fault Studies (JSAF)